energies

MDPI

Article

Closed-Loop Adaptive High-Starting Torque Scalar Control Scheme for Induction Motor Variable Speed Drives

Juan Carlos Travieso-Torres [1,*], Manuel A. Duarte-Mermoud [2,3], Matías Díaz [4], Camilo Contreras-Jara [1] and Francisco Hernández [1]

[1] Department of Industrial Technologies, University of Santiago de Chile, Santiago 9170125, Chile; camilo.contrerasj@usach.cl (C.C.-J.); francisco.hernandezab@usach.cl (F.H.)
[2] Facultad de Ingeniería y Arquitectura, Universidad Central de Chile, Av. Santa Isabel 1186, Santiago 8330601, Chile; manuel.duarte@ucentral.cl
[3] Advanced Mining Technology Center, University of Chile, Av. Tupper 2007, Santiago 8370451, Chile
[4] Department of Electrical Engineering, University of Santiago de Chile, Santiago 9170125, Chile; matias.diazd@usach.cl
* Correspondence: juancarlos.travieso@usach.cl

Abstract: This article proposes a closed-loop (CL) high-starting torque (HST) scalar control scheme (SCS) for induction motors (IM). It endows the recently proposed HST-SCS with high-output torque capability beyond starting after using an outer speed control loop feeding an inner current control loop with adaptive controllers. Presenting a cascade normalized adaptive passivity-based controller (N-APBC) for nonlinear systems encompassing the IM allows obtaining this result. It extends the normalized adaptive controller for the cascade case. As a result, it keeps the HST-SCS simple control scheme without needing variable observers or parameter estimators and employing tuning information only from the motor nameplate and datasheet. Test bench experiments with a 10 HP motor validate the proposal's effectiveness. Comparative experimental results show that the CL HST-SCS has a required stator phase voltage lower than HST-SCS. The CL HST-SCS applies the adaptive starting voltage curve for a more extended time than HST-SCS, from the start to 1.9 s versus 1.2 s, respectively. Hence, CL HST-SCS assures HST not only for starting but almost up to 600 rpm, resulting in a smoother transient behavior than HST-SCS under this speed.

Keywords: adaptive control; induction motors; nonlinear dynamical systems; variable speed drives

Citation: Travieso-Torres, J.C.; Duarte-Mermoud, M.A.; Díaz, M.; Contreras-Jara, C.; Hernández, F. Closed-Loop Adaptive High-Starting Torque Scalar Control Scheme for Induction Motor Variable Speed Drives. *Energies* **2022**, *15*, 3489. https://doi.org/10.3390/en15103489

Academic Editor: Tian-Hua Liu

Received: 4 April 2022
Accepted: 29 April 2022
Published: 10 May 2022

1. Introduction

Variable speed drive (VSD) applications [1] widely use IM [2]. This is due to its lower cost, higher efficiency, and lower maintenance compared with other electric motors.

The VSD performing the scalar control scheme (SCS) [3] mainly moves blowers, fans, and centrifugal pumps [4]. These low-performance applications demand a starting electromagnetic torque of up to 25% of the nominal torque, corresponding to the capacity of the standard SCS. Moreover, the SCS has nonrapid and even oscillatory transient speed behavior with a steady-state speed-accuracy between 1% to 4% for higher speeds [5]. Furthermore, it has the most straightforward control scheme without parameter estimates or variable observers, as shown in Figure 1.

Standard SCS follows the required rotor angular speed ω_r^* after establishing the necessary angular electrical frequency ω_e^* and stator voltage amplitude V_s^*. It applies a boost voltage V_{boost}, adjusted from 3% to 50% of V_{sn}, to assure a starting electromagnetic torque from 0.09% to 25% of the rated torque. It acts at the minimum angular frequency ω_{min}, tuned from 3% to 6% of the rated angular electrical frequency $\omega_{en} = \frac{4\pi f_n}{p}$, to protect the IM from overcurrent consumption. Later, at the cut angular frequency ω_c, tuned from 40% to 50% of ω_{en}, it switches to the V/f curve, which also saturates at the rated voltage for IM protection [6].

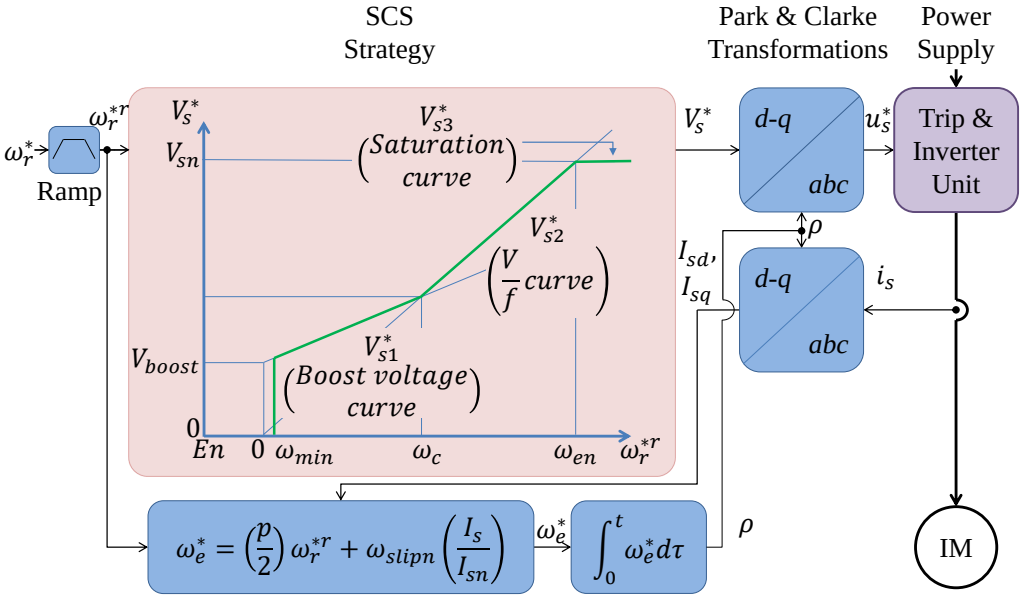

Figure 1. Standard SCS block diagram for IM [6].

Based on previous information, the following sections describe this paper's motivation, background, related work, and claims.

1.1. Motivation

Several researchers aim to improve the SCS scheme. Beyond studying the speed oscillations across the boost voltage curve, the work [5] proposes two methods to mitigate them. To enhance the steady-state accuracy of the actual rotor angular speed, reference [7] uses a closed-loop speed control. Moreover, reference [8] proposes a PI slip controller.

Other proposals develop a slip speed estimator based on an electromagnetic torque estimation in [9], on a gap power estimation in [10], and on a stator flux observer in [11]. Based on the ratio between the rated slip and rated stator current, references [6,12] calculate the slip. Furthermore, the work [13] proposes an optimal V/f ratio based on a reactive power estimate. These proposals require IM parameters or variable estimation, with the exception of [6].

Moreover, other works focus on improving the reduced starting electromagnetic torque SCS issue reported in [14,15]. The solution given in [14] needs stator resistance and a flux estimator. At the same time, the proposal [15] avoids parameters and variable estimators, keeping a simple control scheme. Later, reference [16] gives an alternative solution to the novel method given in [15]. It assures less stator current composition and faster speed response than the standard SCS [6], with no need for the minimum angular frequency ω_{min}.

This paper aims to further improve [16] results, taking into account the following background information.

1.2. Background

The work [15] calls its solution high-starting torque (HST)-SCS. It has a multiple-input and multiple-output (MIMO) APBC that switches to the standard boost voltage curve of the SCS [6], causing curve speed and current chattering issues. The proposal [16] solves these issues after presenting a scalar output normalized APBC that smoothly switches to the standard boost voltage curve of the SCS [6]. As a result, reference [16] expands the applications of the standard SCS [6], including HST capability and keeping a simple control scheme without parameter or variable estimation. It can move, for instance, loaded conveyor belts requiring 100% of the nominal torque at the start and low steady-state speed-accuracy [16].

As an alternative to the APBC controller [16], the work [17] proposes using a normalized MRAC in the HST-SCS with good results. This paper also aims to further improve [16] by suggesting a different adaptive controller. The following section describes the details.

1.3. Related Works

All previously discussed starting adaptive control algorithms are based on the adaptive concepts given in [18] for a model reference adaptive controller (MRAC). The work [15] uses an adaptive passivity-based controller (APBC), reducing the trial and error APBC adjustment given in [19]. Nevertheless, the normalized APBC proposed in [16] further improves the APBC tuning [15] with a solution less dependent on the operational range and motor power. The work [17] proposes using a normalized MRAC, extending the direct approach described in [18].

So far, all HST-SCS, including this paper's proposal, use a pure adaptive controller, active only during starting. Hence, these are not gain scheduling controllers such as the one used in [20] to control a brushless DC motor. This paper extends the cascade APBC proposed in [21] and applies it to the HST-SCS of IM, as the following describes.

1.4. Claims

This paper's main contribution is proposing a CL HST-SCS based on a cascade normalized-APBC (N-APBC). It starts expanding the standard cascade APBC proposed in [21], normalizing the information vector and adaptive law gains for a more straightforward tuning method. Later, the cascade N-APBC design regulates the IM starting stator current decreasing the current consumption, diminishing IM stress and failure risk due to this cause [22]. The solution keeps the simplicity of the SCS, only using tuning information from the motor nameplate and datasheet, not needing variable observers or parameter estimators. It applies the slip speed calculation's industry solution of [6].

This paper's organization is as follows. The Preliminaries Section describes the basic HST-SCS, including its block diagram, control strategy, and method fundamentals. Later, Section 3 describes the proposed CL HST-SCS with the its block diagram, remarking the differences and the closed-loop control strategy. The Experimental Results Section tests both CL HST-SCS and HST-SCS strategies and describes the obtained results. Finally, the Conclusion Section presents the main findings summary.

2. Preliminaries of the Basic HST-SCS

Figure 2 presents the basic HST-SCS block diagram [16].

The basic HST-SCS follows the required rotor angular speed ω_r^* after establishing the required angular electrical frequency ω_e^* and stator voltage amplitude V_s^*. It takes steady-state nominal variable values from the motor nameplate for configuring purposes. For instance, the rated current per phase I_{sn}, the rated voltage per phase V_{sn}, the number of poles p, the electrical frequency f_n, and the rated rotor angular speed ω_{rn}. These last two allow calculating the nominal slip speed ω_{slipn} as follows [6]:

$$\omega_{slipn} = \omega_{en} - \left(\frac{p}{2}\right)\omega_{rn}, \tag{1}$$

which allows computing the actual ω_{slipn} for the required ω_r^* joint to I_{sn} and the actual I_s. This last one is an RMS value obtained from the instantaneous stator components I_{sd} and I_{sq}, considered as sinusoidal signals, and as follows:

$$I_s = \frac{\sqrt{I_{sd}^2 + I_{sq}^2}}{\sqrt{2}}. \tag{2}$$

The required stator voltage amplitude (3) switches from different voltages curves V_{s0}^*, V_{s1}^*, V_{s2}^*, and V_{s3}^* [16] after enabling the VSD ($En = 1$), as the following describes:

$$V_s^* = \begin{cases} V_{s0}^* \text{ (APBC)} & \text{if } En = 1 \& V_{s0}^* < V_{s1}^* \\ V_{s1}^* = \sqrt{2}(P_1\omega_e^* + V_{boost}) & \text{if } V_{s2}^* < V_{s1}^* \leq V_{s0}^* \\ V_{s2}^* = \sqrt{2}P_2\omega_e^* & \text{if } V_{s1}^* < V_{s2}^* \leq V_{s3}^* \\ V_{s3}^* = \sqrt{2}V_{sn} & \text{if } V_{s2}^* > V_{s3}^* \end{cases}. \quad (3)$$

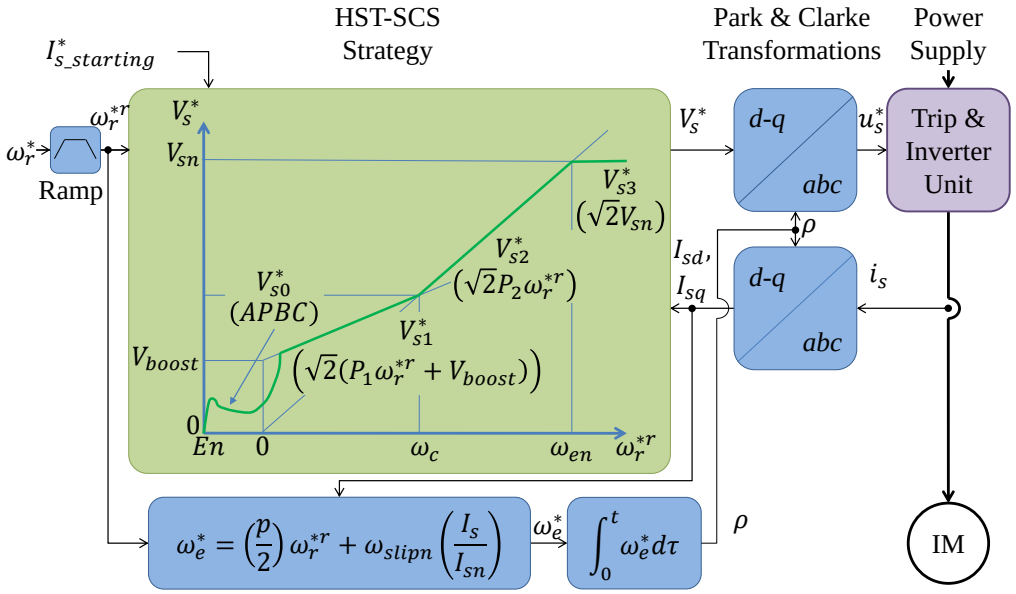

Figure 2. Basic HST-SCS block diagram for IM [16].

Moreover, the required stator voltage amplitude (3) alternates after applying the transformations of Park $e^{j\rho}$ [23] and Clarke [24], detailed in [25]. In [16], the voltage curve V_{s0}^* of (3) aims to keep a constant stator flux magnitude at the start via the following APBC that regulates the starting stator current [16]:

Theorem 1 ([16]). *After applying the following normalized-APBC to the IM d-q model:*

$$\begin{aligned} &V_{s0} = \theta^T \bar{\Omega} \\ &\theta^T = \int_0^t \Gamma e \bar{\Omega}^T d\tau, \text{ with } e = I^*_{s\_starting} - I_{sn}, \text{ and } I^*_{s\_starting} = \xi I_{sn} \\ &\bar{\Omega} = 100 \left[\underbrace{\frac{v}{v_n}}_{\bar{\Omega}_1} \; \underbrace{\frac{I_{sd}}{I_{sn}}}_{\bar{\Omega}_2} \; \underbrace{\frac{I_{sq}}{I_{sn}}}_{\bar{\Omega}_3} \; \underbrace{\frac{\omega_e^* I_{sq}}{\omega_{en} I_{sn}}}_{\bar{\Omega}_4} \; \underbrace{\frac{\omega_r^* I_{sd}}{\omega_{rn} I_{sn}}}_{\bar{\Omega}_5} \; \underbrace{\frac{\omega_r^* I_{sq}}{\omega_{rn} I_{sn}}}_{\bar{\Omega}_6} \right]^T, \\ &\Gamma = \tfrac{\epsilon}{1+100^2}, \text{ and; } \theta^T(0) = 0 \\ &v = Ke \text{ with } K = \tfrac{5m}{\tau_{elect}}, \; \tau_{elect} = \tfrac{\tau_{mech}}{10}, \text{ and } \tau_{mech} = \tfrac{1}{2J_m}, \\ &\text{and } \epsilon \in [0.1, 10], \; m \in [0.1, 10], \xi \in [0.5, 1.5], \; v_n = K, \end{aligned} \quad (4)$$

it turns the IM into a C^1 passive system from e to the auxiliary variable v. It also guarantees that $\lim_{t\to\infty} e = 0$.

This voltage curve V_{s0}^* uses the stator flux magnitude dependence on the magnetizing current, $|\Phi_s| = L_m|i_m|$, considering the incoming expression [15,16]:

$$|\Phi_s| = L_m|i_m| = L_m|i_s - \overbrace{\frac{jL_m}{\frac{R_r}{\omega_{slip}} + jL_r} i_s}^{i_r}| = L_m|i_s\left(\frac{\frac{R_r}{\omega_{slip}} + jL'_r}{\frac{R_r}{\omega_{slip}} + jL_r}\right)|, \quad (5)$$

where L'_r is the rotor leakage inductance, L_m is the magnetizing inductance, and R_r and L_r are the stator resistance and inductance, respectively. Moreover, i_s, i_r, and i_m are the stator, rotor, and magnetizing phase currents, respectively.

Furthermore, regulating the starting stator current i_s guarantees a high starting electromagnetic torque capability as the following describes [15,16]:

$$T_{em} = \overbrace{3\left(\frac{p}{2}\right)\left|\frac{jL_m}{\frac{R_r}{\omega_{slip}} + jL_r}\right|^2}^{K_p} |i_s|^2. \tag{6}$$

The boost voltage curve V^*_{s1} and the V/f voltage curve V^*_{s2}, from Figures 1 and 2, are basically proportional controllers, adjusted as follows:

$$P_1 = \left(\frac{V_{sn}}{\omega_{en}} - \frac{V_{boost}}{\omega_c}\right) \quad \text{and} \quad P_2 = \left(\frac{V_{sn}}{\omega_{en}}\right), \tag{7}$$

The voltage curves V^*_{s1} and V^*_{s2} aim to keep a constant stator flux magnitude $|\Phi_s|$ but using its dependence on the stator voltage and angular electrical frequency ratio $|\Phi_s| \sim \frac{|u_s|}{\omega^*_e}$. This comes from the steady-state IM equivalent circuit per phase after applying Kirchhoff's stator voltage law [3,15,16,25] and neglects the stator impedance voltage drop, as follows:

$$u^*_s = \overbrace{R_s i_s + j\omega^*_e L'_s i_s}^{drop\ voltage \approx 0} + j\omega^*_e \overbrace{L_m i_m}^{\Phi_s} \Rightarrow |\Phi_s| \sim \frac{|u_s|}{\omega^*_e}, \tag{8}$$

where R_s and L'_s are the stator resistance and leakage inductance, respectively. Moreover, u_s is the stator phase voltage. Finally, V^*_{s3} prevents the IM from operating over the nominal stator voltage, V_{sn}, and protects it.

Remark 1. *The APBC (4) proposed in [16] considers the required rotor angular speed instead of the actual rotor angular speed, i.e., $\omega_r = \omega^*_r$, and effectively regulates the stator current around the start. However, the following section extends its efficacy after considering the actual speed and a cascade APBC.*

3. Proposed CL HST-SCS for IM

In this section, based on the following IM dynamical d-q model described, this paper proposes a cascade N-APBC and applies it to HST-SCS.

3.1. Proposed Cascade N-APBC for Nonlinear Systems

The IM dynamical d-q model is a class of nonlinear systems defined as follows:

$$\begin{aligned} \dot{y}_i(t) &= \alpha a(y_i, y_o) + \beta b(y_i, y_o) u_i(t), \\ \dot{y}_0(t) &= \gamma c(y_i, y_o) + \delta d(y_i, y_o) y_i(t), \\ \dot{z}(t) &= q(z, y). \end{aligned} \tag{9}$$

Here, $y_i(t),\ y_o(t) \in \Re$ are the inner and outer outputs; the inner and outer control inputs are $u_i(t),\ y_i(t)^* \in \Re$. The unknown parameters are $\beta,\ \delta \in \Re$, α, and $\gamma \in \Re^{1xn}$. The known nonlinear functions are $b(y_i, y_o),\ d(y_i, y_o) \in \Re$, $a(y_i, y_o)$, and $c(y_i, y_o) \in \Re^m$, with $b(y_i, y_o) \neq 0$ and $d(y_i, y_o) \neq 0$. Moreover, it has a bounded-input bounded-output (BIBO) internal dynamics $z(t) \in \Re^l$.

The following Theorem 2 extends a cascade APBC [21] for nonlinear systems of the form (9).

Theorem 2. *After applying the following cascade N-APBC to the nonlinear system (9), it turns the IM into a C^1 passive system from e_o and e_i to the auxiliary variables v_0 and v_i, respectively,*

with $e_o(t) = y_o^*(t) - y_o(t)$ *and* $e_i(t) = y_i^*(t) - y_i(t)$. *It also guarantees that* $\lim_{t\to\infty} e_o = 0$ *and* $\lim_{t\to\infty} e_i = 0$

$$
\begin{aligned}
&\text{Inner Loop}\\
&u_i(t) = b(y_i, y_o)^{-1}\theta_i(t)^T\overline{\Omega_i(t)}, && \text{adaptive controller}\\
&\theta_i^T = \int_0^t \Gamma_i e_i \overline{\Omega_i(t)}^T d\tau, \text{ with } \theta_i^T(0) = 0, && \text{adaptive controller parameter}\\
&\overline{\Omega_i(t)}^T = 100\begin{bmatrix} \overbrace{\frac{a(y_i,y_o)}{a_n}}^{\overline{a(y_i,y_o)}} & \overbrace{\frac{v_i(t)}{K_i}}^{\overline{v_i(t)}} \end{bmatrix}, && \text{normalized information vector}\\
&\text{with } \Gamma_i = \tfrac{\epsilon_i}{1+100^2}, && \text{normalized fixed gain}\\
&\text{and } v_i(t) = K_i e_i + \dot{y}_i^*(t), && \text{inner auxiliary variable}
\end{aligned}
\tag{10}
$$

$$
\begin{aligned}
&\text{Outer Loop}\\
&y_i^*(t) = d(y_i, y_o)^{-1}\theta_o(t)^T\overline{\Omega_o(t)}, && \text{adaptive controller}\\
&\theta_o^T = \int_0^t \Gamma_o e_o \overline{\Omega_o(t)}^T d\tau, \text{ with } \theta_o^T(0) = 0, && \text{adaptive controller parameter}\\
&\overline{\Omega_o(t)}^T = 100\begin{bmatrix} \overbrace{\frac{c(y_i,y_o)}{c_n}}^{\overline{c(y_i,y_o)}} & \overbrace{\frac{v_o(t)}{K_i}}^{\overline{v_o(t)}} \end{bmatrix}, && \text{normalized information vector}\\
&\text{with } \Gamma_0 = \tfrac{\epsilon_o}{1+100^2}. && \text{normalized fixed gain}\\
&\text{and } v_o(t) = \xi^{-1}K_i e_o + \dot{y}_o^*(t), && \text{outer auxiliary variable}
\end{aligned}
\tag{11}
$$

Here, $y_o^*(t)$ *is the desired trajectory. The normalization factors* a_n, c_n, y_n, *and* y_n^* *correspond to the maximum operational range of* $a(y)$, $c(y)$, $y(t)$, *and* $y^*(t)$, *respectively. The normalized information vectors consider these factors and multiply by* 100, *normalizing a* 100 *range. Hence, the fixed-gains* Γ_i, Γ_0, *and* $\in \Re^+$ *have a form* $\frac{\epsilon}{1+\xi^2}$ *[16], with* $\xi = 100$. *Then, these use the term* $\frac{1}{1+100^2}$ *for a fast tuning, assuring a reasonable operating range and the design parameters* $\epsilon_i, \epsilon_o \in [0.1, 10]$, *which allows a fine-tuning adjustment. Moreover,* $\xi \in [3, 10]$ *assures an inner loop* ξ *times faster than the outer loop for the cascade proper functioning. Appendix A contains the stability proof of Theorem 1.*

The following section applies Theorem 2 to the IM and describes the proposal details.

3.2. Cascade N-APBC Applied to HST-SCS for IM

Figure 3 shows the proposed CL HST-SCS block diagram for IM.

It has a similar control scheme to Figure 2 but adjusts the voltage curve V_{s0}^* after applying the proposed cascade N-APBC (10, 11) to the IM model, once considering as unknown its nonlinear parameters α, β, γ, and δ, and its known functions $a(y)$, $b(y)$, $c(y)$, and $d(y)$. Hence, the proposal also uses (1) to calculate the slip. However, it establishes the scalar required stator voltage V_s^* (3), replacing the adaptive controller (4) conforming the voltage curve V_{s0}^* with the following proposed controller for V_{s0}^*.

Inner Loop

$$V_{s0} = \theta_i^T \bar{\Omega}_i, \text{where } \theta_i^T = \int_0^t \Gamma_i e_i \bar{\Omega}_i^T d\tau,$$

$$\bar{\Omega}_i = 100 \left[\underbrace{\frac{\bar{\Omega}_{i1}}{\frac{v_i}{K_i}}} \; \underbrace{\frac{\bar{\Omega}_{i2}}{\frac{I_{sd}}{I_{sn}}}} \; \underbrace{\frac{\bar{\Omega}_{i3}}{\frac{I_{sq}}{I_{sn}}}} \; \underbrace{\frac{\bar{\Omega}_{i4}}{\frac{\omega_e^* I_{sq}}{\omega_{en} I_{sn}}}} \; \underbrace{\frac{\bar{\Omega}_{i5}}{\frac{\omega_r I_{sd}}{\omega_{rn} I_{sn}}}} \; \underbrace{\frac{\bar{\Omega}_{i6}}{\frac{\omega_r I_{sq}}{\omega_{rn} I_{sn}}}} \right]^T, \tag{12}$$

with $\Gamma_i = \frac{\epsilon_i}{1+100^2}$, $\theta_i^T(0) = 0$,
and $v_i = K_i e_i + \dot{I}_{sd}^*$, with $K_i = \frac{5m}{\tau_{elect}}$, $\tau_{elect} = \frac{\tau_{mech}}{10}, \tau_{mech} = \frac{1}{2Jm}$,
here, $e_i = I_{sd}^* - I_{sd}$.

Outer Loop

$$I_{sd}^* = Sign(\theta_o^T \bar{\Omega}_o) \sqrt{|\, \theta_o^T \bar{\Omega}_o \,|} + I_{s\_starting}^*$$

$$\text{where } \theta_o^T = \int_0^t \Gamma_o e_o \bar{\Omega}_o^T d\tau, \; \bar{\Omega}_o = 100 \left[\underbrace{\frac{\bar{\Omega}_{o1}}{\frac{v_o}{K_i}}} \; \underbrace{\frac{\bar{\Omega}_{o2}}{\frac{\omega_r}{\omega_{rn}}}} \; \underbrace{\frac{\bar{\Omega}_{03}}{1}} \right]^T, \tag{13}$$

with $\Gamma_o = \frac{\epsilon_o}{1+100^2}$, $\theta_o^T(0) = 0$,
$v_o = \xi^{-1} K_i e_o + \dot{\omega}_r^*$, and $e_o = \omega_r^* - \omega_r$.

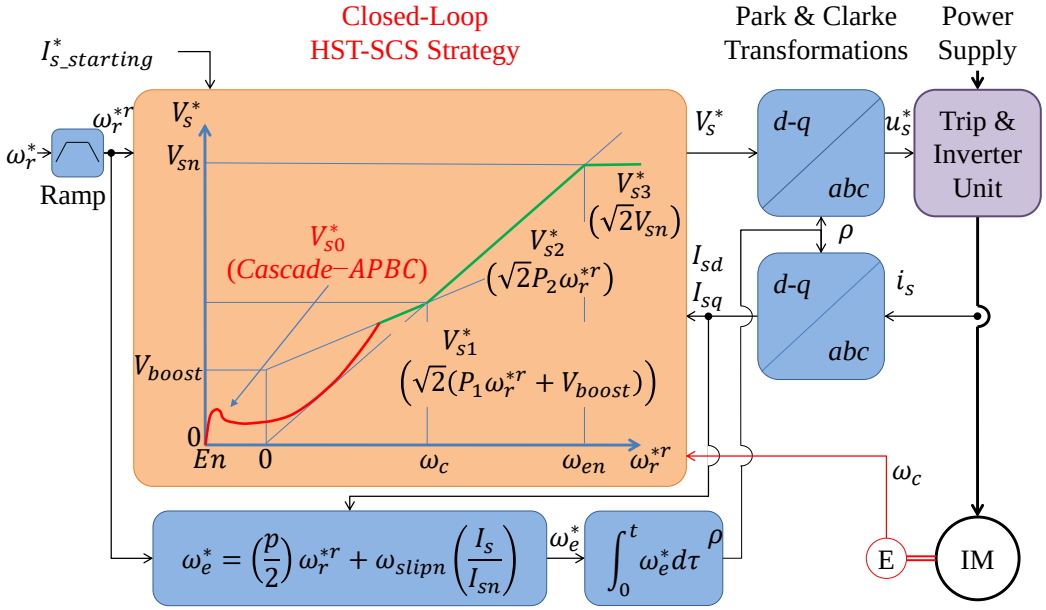

Figure 3. Block diagram of the proposed CL HST-SCS for IM, remarking the differences in red.

Here, the adaptive controller parameters are $\theta_i \in \Re^6$ and $\theta_o \in \Re^3$. The fixed-gains are Γ_i, $\Gamma_o \in \Re^+$ depending on the design parameter $\epsilon_o, \epsilon_i \in [0.1, 10]$. The normalized information vectors are $\bar{\Omega}_i \in \Re^6$ and $\bar{\Omega}_o \in \Re^3$.

The CL HST-SCS considers that the IM dynamical d-q model has the form of (9). Here, the outputs are $y_i(t) = I_{sd}, y_o(t) = \omega_r \in \Re$, and the control inputs are $u_i(t) = V_{sd}, u_o(t) = |I_s|^2 \in \Re$. The unknown parameters are $\alpha = \left[A_{1upper}\ 1\ A_{2upper}\right] \in \Re^5$, $\beta = \frac{1}{\sigma L_s}$, $\gamma = \left[-\frac{b_p}{J}\ \frac{1}{J}T_l\right] \in \Re^2$, and $\delta = |\frac{jL_m}{\frac{R_r}{\omega_{slip}} + jL_r}|^2$. Additionally, the known nonlinear functions are $a(y) = \left[I_{sd}\ I_{sq}\ \omega_e^* I_{sq}\ \frac{p}{2}\omega_r I_{sq}\ \frac{p}{2}\omega_r I_{sq}\right]^T \in \Re^5$, $b(y) = 1$, $c = [\omega_r\ 1]^T \in \Re^2$, and $d = \frac{3p}{2}$. Moreover, the internal dynamics are $z(t) = \left[I_{sq}\ \Phi_{rd}\ \Phi_{rq}\right]^T \in \Re^3$, defined as follows:

$$q(z,y) = \begin{bmatrix} A_{1lower}\begin{bmatrix} I_{sd} \\ I_{sq} \end{bmatrix} - \omega_e^* I_{sd} + A_{2lower}\frac{p}{2}\omega_r \begin{bmatrix} I_{sd} \\ I_{sq} \end{bmatrix} + \beta V_{sq} \\ C\begin{bmatrix} \Phi_{rd} \\ \Phi_{rq} \end{bmatrix} + d\begin{bmatrix} I_{sd} \\ I_{sq} \end{bmatrix} \end{bmatrix}. \tag{14}$$

Here, Φ_{rd} and Φ_{rq} are the rotor flux direct and quadrature components, respectively. The mechanical viscous damping is b_p, the motor-load inertia is J, and the load torque is T_l. Moreover, the vector $A_{1upper} \in \Re^2$ and $A_{1lower} \in \Re^2$ are upper and lower rows of the matrix A_1, respectively. The vectors $A_{2upper} \in \Re^2$ and $A_{2lower} \in \Re^2$ are the upper and lower rows of matrix A_2, respectively. Moreover, C, d, A_1, and A_2 are defined as follows [16]:

$$\begin{aligned} C &= \begin{bmatrix} -\frac{R_r}{L_r} & \omega_{slip} \\ -\omega_{slip} & -\frac{R_r}{L_r} \end{bmatrix},\ d = \frac{R_r L_m}{L_r}, \\ A_1 &= \begin{bmatrix} -\frac{R_s'}{\sigma L_s} & 0 \\ 0 & -\frac{R_s'}{\sigma L_s} \end{bmatrix} - \frac{L_m R_r}{\sigma L_s L_r^2} d C^{-1},\ A_2 = -\frac{L_m R_r}{\sigma L_s L_r} d \begin{bmatrix} 0 & 1 \\ -1 & 0 \end{bmatrix} C^{-1}. \end{aligned} \tag{15}$$

Furthermore, σ is the leakage or coupling coefficient, given by $\sigma = 1 - L_m^2/(L_r L_s)$, and R_s' is the stator transient resistance, with $R_s' = R_s + (L_m^2 R_r)/(L_r^2)$.

The following Algorithm 1 contains the pseudocode of the proposed CL HST-SCS. Here, the required stator voltage amplitude (3) considers the proposed cascade-APBC (12) and (13).

Algorithm 1 Pseudocode of the required voltage and frequency for the CL HST-SCS

Require: ω_r^*, $I_{s\_starting}^*$, E_n (Reference and Input Signal)
Require: p, J_m, f_n, ω_{rn}, I_{sn}, V_{sn},, ω_c, m, ϵ_i, ϵ_i, ξ, $ramp\_rate$ (Configuring Parameters)
Require: ω_r, I_{sd}, I_{sq} (Measurements)
Ensure: Required Stator Voltage V_s^* and electrical frequency ω_e^*

ω_e^* **Calculus**

$$\omega_{en} = \frac{4\pi f_n}{p};\ \ \omega_{slipn} = \omega_{en} - \left(\frac{p}{2}\right)\omega_{rn};\ \ I_s = \frac{\sqrt{I_{sd}^2 + I_{sq}^2}}{\sqrt{2}};\ \ \omega_r^{*r} = \textbf{Ramp}(\omega_r^*, ramp\_rate);$$

$$\omega_e^* = \left(\frac{p}{2}\right)\omega_r^{*r} + \omega_{slipn}\left(\frac{I_s}{I_{sn}}\right);$$

V_{s0} **Computing**

Outer Loop

Compute: $e_o = \omega_r^* - \omega_r;\ \ \tau_{mech} = \frac{1}{2J_m};\ \ \tau_{elect} = \frac{\tau_{mech}}{10};\ \ K_i = \frac{5m}{\tau_{elect}};$

$$v_o = \xi K_i e_o + \dot{\omega}_r^*;\ \ \Gamma_o = \frac{\epsilon_o}{1+100^2};$$

$$\bar{\Omega}_o = 100\left[\underbrace{\frac{v_o}{\xi K_i}}_{\bar{\Omega}_{o1}}\ \underbrace{\frac{\omega_r}{\omega_{rn}}}_{\bar{\Omega}_{o2}}\ \underbrace{1}_{\bar{\Omega}_{03}}\right]^T;\ \ \theta_o^T = \int_0^t \Gamma_o e_o \bar{\Omega}_o^T d\tau;$$

$$I_{sd}^* = Sign(\theta_o^T \bar{\Omega}_o)\sqrt{|\ \theta_o^T \bar{\Omega}_o\ |} + I_{s\_starting}^*;$$

Inner Loop

Compute: $e_i = I_{sd}^* - I_{sd};\ \ v_i = K_i e_i + \dot{I}_{sd}^*;\ \ \Gamma_i = \frac{\epsilon_i}{1+100^2};$

$$\bar{\Omega}_i = 100\left[\underbrace{\frac{v_i}{K_i}}_{\bar{\Omega}_{i1}}\ \underbrace{\frac{I_{sd}}{I_{sn}}}_{\bar{\Omega}_{i2}}\ \underbrace{\frac{I_{sq}}{I_{sn}}}_{\bar{\Omega}_{i3}}\ \underbrace{\frac{\omega_e^* I_{sq}}{\omega_{en} I_{sn}}}_{\bar{\Omega}_{i4}}\ \underbrace{\frac{\omega_r I_{sd}}{\omega_{rn} I_{sn}}}_{\bar{\Omega}_{i5}}\ \underbrace{\frac{\omega_r I_{sq}}{\omega_{rn} I_{sn}}}_{\bar{\Omega}_{i6}}\right]^T;$$

$$\theta_i^T = \int_0^t \Gamma_i e_i \bar{\Omega}_i^T d\tau;\ \ V_{s0} = \theta_i^T \bar{\Omega}_i;$$

Algorithm 1 *Cont.*

V_{s1} **Computing**
Compute: $V_{s1}^* = \sqrt{2}(P_1\omega_e^* + V_{boost})$;

V_{s2} **Computing**
Compute: $V_{s2}^* = \sqrt{2}P_2\omega_e^*$;

V_{s3} **Computing**
Compute: $V_{s3}^* = \sqrt{2}V_{sn}$;

Voltage Curve Selection

if $En = 1$ **and** $V_{s0}^* < V_{s1}^*$ **then**
$V_s^* = V_{s0}^*$
else if $V_{s2}^* < V_{s1}^* \leq V_{s0}^*$ **then**
$V_s^* = V_{s1}^*$
else if $V_{s1}^* < V_{s2}^* \leq V_{s3}^*$ **then**
$V_s^* = V_{s2}^*$
else $V_{s2}^* > V_{s3}^*$
$V_s^* = V_{s3}^*$
end if

The following section describes the proposal's experimental results.

4. Comparative Experimental Results

This section describes the test bench used to validate the proposal, the experimental setup, and the comparative results.

4.1. Test Bench Characteristics

Figure 4 illustrates the test bench used for the comparative experimental results, considering the basic HST-SCS and the CL HST-SCS. The programming of these strategies uses Simulink version 8.9, Matlab R2017a running on PC. Both consider a pulse width modulation (PWM) switching at 8 kHz. Once finished, the PC downloads them via a UTP cable to the control platform. It is a real-time simulator controller OPAL-RT 4510 v2 giving the trip pulses to a two-level inverter unit feeding an IM-load assembly with the parameters of Table 1. The power supply feeds the inverter through a variac.

Remark 2. *The used test bench is based on a double-edge naturally sampled PWM with a two-level voltage source inverter [26], which inherently produces a bipolar switching pattern at the converter outputs. However, the control proposal could also be implemented using the space vector modulation method to improve the harmonic content further, especially for higher modulation indexes when the machine operates around the rated speed [26,27]. The proposed CL HST-SCS could also be implemented in a three-level converter using unipolar PWM.*

Table 1. Data from the motor nameplate and datasheet.

Symbol	Quantity	Values
P_n	rated output power	7.5 kW
V_{sn}	rated phase voltage	220 V
I_{sn}	rated phase current	15.5 A
PF_n	rated power factor	0.85
f_n	rated electrical frequency	50 Hz
p	poles number	4
ω_{rn}	rated rotor angular speed	152 rad/s
J_m	motor inertia (data-sheet)	0.2 kgm/s^2

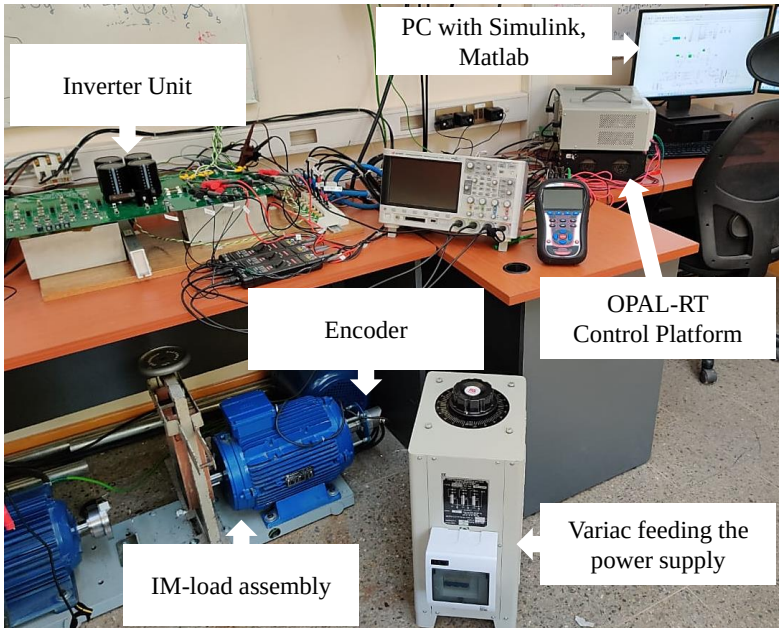

Figure 4. Picture of the testing bench.

From this Table 1, the following parameters are calculated: the rated electrical frequency $\omega_{en} = \frac{4\pi f}{p} = 314.16$ rad/s and the rated electromagnetic torque $T_n = \frac{1000P_n}{\omega_{rn}} = 49.2$ Nm.

Remark 3. *Please note that IM parameter values, such as L_r, L_s, L_m, R_r, and R_s, are unknown. Moreover, their knowledge is unnecessary for the proposed CL HSTSCS configuring. Not even the torque-speed characteristic of the feed IM is needed. Table 1 shows the only required IM information taken from the motor nameplate and datasheet.*

The following section describes the experimental testing setup.

4.2. Experimental Setup

The same testing applies to both strategies, the basic HST-SCS [16] and CL HST-SCS. It considers the IM has a nominal torque load (set by a prony brake), a 6-second duration test, enabling the VSDs at 0.3 s, and applying a step speed command of 200 rpm, 100 rpm, 1450 rpm, 1300, and 1150 rpm, at times 1 s, 1.4 s, 1.7 s, 4 s, and 5 s, respectively. The prony brake adjustment is 49.6 Nm at the rated speed of 1455 rpm. As a result, the load torque equals 49.2 Nm (the rated torque) at 200 rpm and 100 rpm, 49.8 Nm at 1455 rpm, 49.6 Nm at 1300 rpm, and 49.4 NM at 1100 rpm.

Table 2 presents the tuning parameters.

Table 2. Tuning parameters for basic HST-SCS [16] versus CL HST-SCS.

Tuning Parameter	Basic HST-SCS [16]	CL HST-SCS
V_{boost}	$40\%V_{sn}$	$40\%V_{sn}$
ω_c	$50\%\omega_{en}$	$50\%\omega_{en}$
K_i	$150J_m$	$150J_m$
Γ_i,	$\frac{1}{1+100^2}$	$\frac{1}{1+100^2}$
Γ_o	—	$\frac{1}{1+100^2}$
$I^*_{s\_starting}$	$\sqrt{2}I_{sn}$	$\sqrt{2}I_{sn}$
m	1	1
ϵ_i	1	1
ϵ_o	—	1
ξ	—	3
$Ramp\_rate$	83.8 rad/s	83.8 rad/s

The following section describes the obtained results.

4.3. Comparative Experimental Results

Figures 5 and 6 show the previous HST-SCS [16] and CL HST-SCS oscilloscope waveforms, respectively. Both figures exhibit the applied line Voltage u_{sab} and the consumed stator phase currents i_{sa}, i_{sb}, and i_{sc} around 5.1 s.

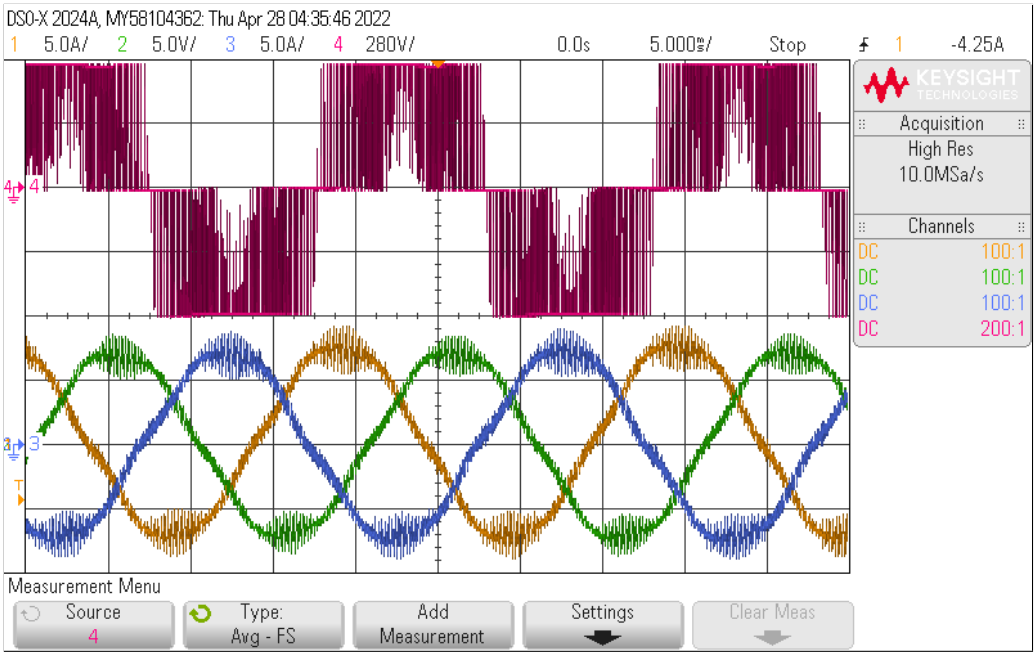

Figure 5. Oscilloscope voltage and current waveforms for the basic HST-SCS [16].

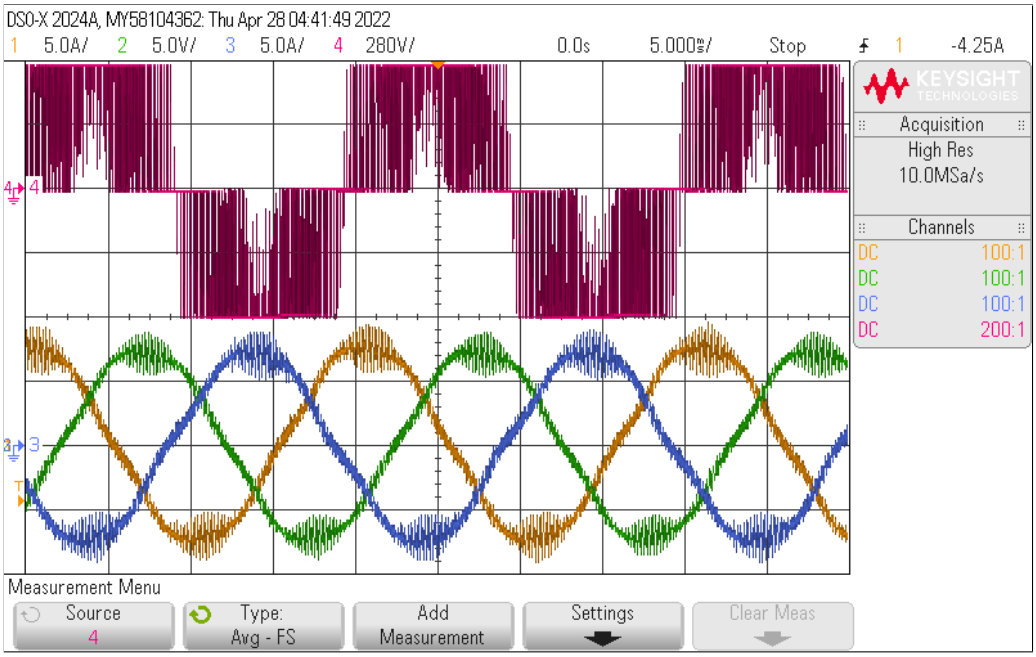

Figure 6. Oscilloscope voltage and current waveforms for the CL HST-SCS.

Below, Figure 7 shows comparative graphics obtained via the OPAL-RT measurements. It displays the consumed stator phase A current i_{sa} joint to the required stator phase voltage amplitude V_s^*, and the rotor angular speed ω_r^* versus ω_r for the basic and CL HST-SCS.

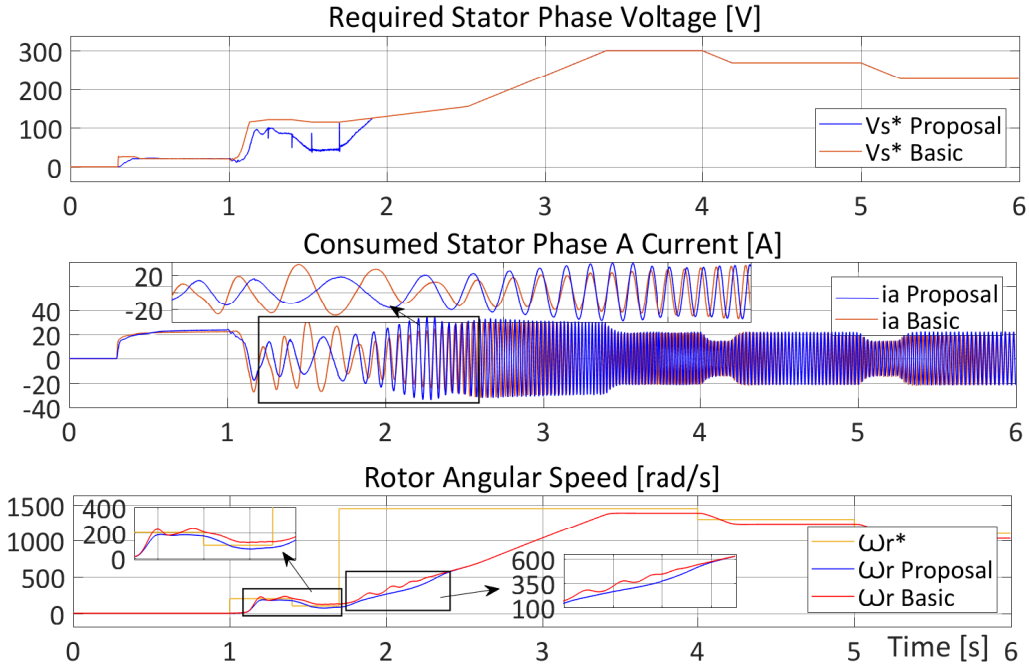

Figure 7. Compararative OPAL-RT waveforms of voltage, current, and rotor angular speed.

The required stator phase voltage V_s^* in Figure 7 shows that CL HST-SCS and HST-SCS apply DC voltage after enabling the VFD and until 1 s. When the IM starts rotating, the HST-SCS keeps using the adaptive starting controller, between 1 s and 1.2 s. Later, it switches to the boost curve, active from 1.1 s to 2.5 s. Finally, the V/f curves operate from 2.5 s until the end.

Figure 7 evidences that required stator phase voltage is lower for the CL HST-SCS. Moreover, the V_{s0} voltage curve applies for a more extended time, from the start to 1.9 s, for the CL HST-SCS. As a result, the CL HST-SCS assures HST not only for starting but almost up to 500 rpm.

The consumed stator phase A current described in Figure 7 displays similarly consumed DC stator current magnitudes (starting currents) for both strategies. These consume 21.9 A for starting; the nominal stator current $\sqrt{2}I_{sn}$. However, it is lower for the CL HST-SCS when starting. After 2.6 s, consumption is similar for the CL HST-SCS and HST-SCS. Figure 7 shows the details.

The actual rotor speed follows the required rotor speed for both HST-SCS strategies. However, the CL HST-SCS has a smoother transient behavior than HST-SCS under 600 rpm. This last one shows a more oscillatory behavior. CL HST-SCS and HST-SCS have similar transient behavior and steady-state accuracy for higher speed references. These last ones are 3.0% for 1455 rpm, 3.8% for 1300 rpm, and 4.1% for 1150 rpm.

The following section describes the conclusions.

5. Conclusions

This paper studies a basic HST-SCS and a CL HST-SCS. Both strategies assure HST with low current consumption compared with the standard SCS [16]. They all follow the required speed. Moreover, they have a simple control scheme without parameters estimation nor variable observers, but only depend on the IM nameplate and datasheet for their configuring.

Comparative experiments were performed on a test bench. These show that the CL HST-SCS delivers high torque capabilities beyond the starting. Thus, CL HST-SCS has a smoother transient behavior than HST-SCS under 600 rpm.

The proposal of a cascade N-APBC for nonlinear systems encompassing IM allows for obtaining the CL HST-SCS. It considers normalized inner and outer adaptive loops

expanding [21]. Moreover, it further extends the APBC [15], normalized in [16], to reduce trial and error APBC adjustment.

The proposed CL HST-SCS contributes to expanding the standard SCS low-performance applications. Not only moving blowers, fans, and centrifugal pumps, but other loads that need a starting torque of 100% rated torque. Future work will consider developing real-time simulations for a higher power IM, including multilevel inverters and SVM modulation.

Author Contributions: Conceptualization, methodology, writing—original draft preparation, and visualization, J.C.T.-T.; investigation, formal analysis, supervision, project administration, data curation, and resources and funding acquisition, J.C.T.-T. and M.A.D.-M.; validation, software, and writing—review and editing; M.D., C.C.-J. and F.H. All authors have read and agreed to the published version of the manuscript.

Funding: This research was funded by FONDEF Chile, grant ID 17I20338; the applied research project DICYT, grant 082078TT_TEC, Vicerrectoría de Investigación, Desarrollo e Innovación; FONDECYT Chile, grant 1190959. Moreover, it was supported by a 2021 research grant from the Technological Faculty, USACH.

Institutional Review Board Statement: Not applicable.

Informed Consent Statement: Not applicable.

Data Availability Statement: Not applicable.

Conflicts of Interest: The authors declare no conflict of interest.

Abbreviations

The following abbreviations are used in this manuscript:

IM	Induction motors
PC	Personal computer
HST	High starting torque
SCS	Scalar control scheme
APBC	Adaptive passivity-based controller
MRAC	Model reference adaptive controller
MIMO	Multiple-input multiple-output
BIBO	Bounded-input bounded-output
FOC	Field-oriented control
PWM	Pulse width modulation
IAE	Integral absolute error
VSD	Variable speed drives
DC	Direct current
SVM	Space vector modulation

Main Notation

The following main notations are used in this manuscript:

ω_r^*, ω_r, and ω_e^*	Required rotor, actual, and electrical angular speed
ω_{rn} and ω_{en}^*	Rated rotor and required angular speed
ω_{slip} and ω_{slipn}	Actual and rated angular slip speed
$e^{-j\rho}$ and $e^{-j\rho}$	Park transformation and its inverse
$T_{3\to2}$ and $T_{2\to3}$	Clarke transformation and its inverse
V_s^*	Needed stator voltage amplitude
$V_{s\alpha\beta}^*$	Needed two-phase alternating instantaneous voltage in α-β coordinates
u_s^*	Needed three-phasic alternating instantaneous voltage
V_{sn}	Rated voltage per phase (RMS value)
I_{sn} and I_s	Rated and actual current per phase (RMS value)
I_{sd} and I_{sq}	Actual stator current direct and quadrature component per phase
i_s, i_r, and i_m	Stator, rotor, and magnetizing instantaneous current
PF_n	Rated power factor
f_n	Rated electrical frequency in Hz

p	Number of poles
En	VFD enable
V_{boost}	boost voltage
V_{s0}^*	Starting voltage curve for HST
V_{s1}^*	Boost voltage curve
V_{s2}^*	V/f voltage curve
V_{s3}^*	Weakening flux zone voltage curve
P_1 and P_2	Controller parameters for V_{s1}^* and V_{s2}^*, respectively
ω_c	Cut angular frequency, switching point between V_{s1}^* and V_{s2}^*
R_s and R_r	Stator and rotor resistance
L_s' and L_r'	Stator and rotor leakage inductance
L_s, L_r, and L_m	Stator, rotor, and magnetizing inductance
σ	Leakage or coupling coefficient, given by $\sigma = 1 - L_m^2/(L_r L_s)$
R_s'	Stator transient resistance, with $R_s' = R_s + (L_m^2 R_r)/(L_r^2)$
$\lvert\Phi_s\rvert$	Stator flux magnitude

Appendix A. Stability Proof of Theorem 1

Proof of Theorem 1. Adding and subtracting the terms $K_i e_i + \dot{y}_i^*$ and $K_o e_o + \dot{y}_o^*$ into the right side of the first and fourth equations of (9), considering that $\dot{e}_i(t) = \dot{y}_i(t) - \dot{y}_i^*(t)$ and $\dot{e}_o(t) = \dot{y}_o(t) - \dot{y}_o^*(t)$, and making some algebraic arrangements, it is obtained that

$$\begin{array}{l} \dot{e}_i(t) = -K_i e_i + \beta\left(\theta_i^{*T}\bar{\Omega}_i - u_i(t)^*\right) \\ \dot{e}_o(t) = -K_o e_o + \delta\left(\theta_o^{*T}\bar{\Omega}_o - I_{sd}^{*2}\right) \\ \dot{z}(t) = q(z,y). \end{array} \tag{A1}$$

where $\theta_i^{*T} = \beta^{-1}\frac{\Omega_{in}}{100}[\alpha\ 1] \in \Re^{(m+1)}$ and $\theta_o^{*T} = \delta^{-1}\frac{\Omega_{0n}}{100}[\gamma\ 1] \in \Re^{(m+1)}$ are the normalized ideal controller parameters. The $Sign(\beta) = 1$ and $Sign(\delta) = 1$ (are positive). All parameters are assumed to be unknown and constant, which may have a slow variation. Thus, the authors substitute (10) and (11) into (A1), and define the controller parameters errors as $\Phi_i = \theta_i^{*T} - \theta_i$ and $\Phi_o = \theta_o^{*T} - \theta_o$ (which implies that $\dot{\Phi}_i(t) = -\dot{\theta}_i(t)$ and $\dot{\Phi}_o(t) = -\dot{\theta}_o(t)$ as θ_i^{*T} and θ_o^{*T} are constant vectors). Moreover, considering stable internal dynamics, as the state variables I_{sq}, Φ_{rd}, and Φ_{rq} are the bounded-input bounded-output (BIBO), the obtained error model is

$$\begin{array}{l} \dot{e}_i(t) = -K_i e_i + b\Phi_i^T\bar{\Omega}_i \\ \dot{\Phi}_i^T(t) = -\Gamma_i e_i \bar{\Omega}_i^T \ \text{ with } \ \Gamma_i \in \Re^+ \\ \dot{e}_o(t) = -K_o e_o + \frac{1}{7}K_p\Phi_o^T\bar{\Omega}_o \\ \dot{\Phi}_o^T(t) = -\Gamma_o e_o \bar{\Omega}_o^T \ \text{ with } \ \Gamma_o \in \Re^+ \end{array} . \tag{A2}$$

The obtained error model (A2) has the following associated Lyapunov function:

$$V(e_i, e_0, \Phi_i, \Phi_o) = \tfrac{1}{2}\left(e_i^2 + e_o^2\right) + \tfrac{1}{2}Trace\Big(\mid\beta\mid\Phi_i^T\Gamma_i^{-1}\Phi_i + \mid\delta\mid\Phi_o^T\Gamma_o^{-1}\Phi_o\Big). \tag{A3}$$

Taking the time derivative of this Lyapunov function we have:

$$\dot{V}(e_i, e_0, \Phi_i, \Phi_o) = e_i\dot{e}_i + e_o\dot{e}_o + Trace\big(\mid\beta\mid\dot{\Phi}_i^T\Gamma^{-1}\Phi_i\big) + Trace\big(\mid\delta\mid\dot{\Phi}_o^T\Gamma_o^{-1}\Phi_o\big). \tag{A4}$$

The time derivatives of e_i, e_o, Φ_i, and Φ_o from (A2) are substituted into this last expression. Moreover, the two vectors' property, where $a^T b = Trace(ab^T)$, is considered to write the terms $e_i\beta\Phi_i^T\Omega_i$ and $e_o\delta\Phi_o^T\Omega_o$ into the trace as $Trace(\beta e_i\Omega_i^T\Phi_i)$ and $Trace(\delta e_o\Omega_o^T\Phi_o)$, respectively. Finally, rearranging and canceling terms due to $\beta = \mid\beta\mid$ and $\delta = \mid\delta\mid$, after knowing both have a positive sign, we obtain:

$$\dot{V}(e_i, e_0, \Phi_i, \Phi_o) = -K_i e_i^2 - K_o e_o^2 \ . \tag{A5}$$

As can be seen in this last Equation (A5), the first time derivative of the Lyapunov function (A3) is negative semidefinite; thus, the autonomous system (A2) is stable. Moreover,

as e_i, e_o, Φ_i, and Φ_o are stables, with bounded Ω_i and Ω_o, then $\dot{e}_i$ and $\dot{e}_o$ are bounded. Integrating both sides of (A5), it can be concluded that $e \in \ell^2$. Hence, according to Barbalat's Lemma, the error e is asymptotically stable. This concludes the proof. □

References

1. Bose, B. *Modern Power Electronics and AC Drives*; Eastern Economy Edition; Prentice Hall PTR: Hoboken, NJ, USA, 2002.
2. Hannan, M.; Ali, J.A.; Mohamed, A.; Hussain, A. Optimization techniques to enhance the performance of induction motor drives: A review. *Renew. Sustain. Energy Rev.* **2018**, *81*, 1611–1626. [CrossRef]
3. Vas, P. *Electrical Machines and Drives: A Space-Vector Theory Approach*; Oxford University Press: New York, NY, USA, 1992.
4. Varma, G.H.K.; Barry, V.R.; Jain, R.K. A Total-Cross-Tied-Based Dynamic Photovoltaic Array Reconfiguration for Water Pumping System. *IEEE Access* **2022**, *10*, 4832–4843. [CrossRef]
5. Carbone, L.; Cosso, S.; Kumar, K.; Marchesoni, M.; Passalacqua, M.; Vaccaro, L. Stability Analysis of Open-Loop V/Hz Controlled Asynchronous Machines and Two Novel Mitigation Strategies for Oscillations Suppression. *Energies* **2022**, *15*, 1404. [CrossRef]
6. Control-Techniques. *Commander SE Advanced User Guide*; Part Number: 0452-0049, Issue Number 3; Control Techniques Drives Limited: Stafford Park, UK, 2002.
7. Otkun, Ö. Scalar Speed Control of Induction Motors with Difference Frequency. *J. Polytech.* **2019**, *23*, 267–276. [CrossRef]
8. Duranay, Z.; Guldemir, H.; Tuncer, S. Implementation of a V/f Controlled Variable Speed Induction Motor Drive. *EMITTER Int. J. Eng. Technol.* **2020**, *8*, 35–48. [CrossRef]
9. Koga, K.; Ueda, R.; Sonoda, T. Constitution of V/f control for reducing the steady-state speed error to zero in induction motor drive system. *IEEE Trans. Ind. Appl.* **1992**, *28*, 463–471. [CrossRef]
10. Munoz-Garcia, A.; Lipo, T.; Novotny, D. A new induction motor V/f control method capable of high-performance regulation at low speeds. *IEEE Trans. Ind. Appl.* **1998**, *34*, 813–821. [CrossRef]
11. Wang, C.C.; Fang, C.H. Sensorless scalar-controlled induction motor drives with modified flux observer. *IEEE Trans. Energy Convers.* **2003**, *18*, 181–186. [CrossRef]
12. Smith, A.; Gadoue, S.; Armstrong, M.; Finch, J. Improved method for the scalar control of induction motor drives. *IET Electr. Power Appl.* **2013**, *7*, 487–498. [CrossRef]
13. Lee, K.; Han, Y. Reactive-Power-Based Robust MTPA Control for v/f Scalar-Controlled Induction Motor Drives. *IEEE Trans. Ind. Electron.* **2022**, *69*, 169–178. [CrossRef]
14. Zhang, Z.; Bazzi, A.M. Robust Sensorless Scalar Control of Induction Motor Drives with Torque Capability Enhancement at Low Speeds. In Proceedings of the 2019 IEEE International Electric Machines Drives Conference (IEMDC), San Deigo, CA, USA, 12–15 May 2019; pp. 1706–1710. [CrossRef]
15. Travieso-Torres, J.C.; Vilaragut-Llanes, M.; Costa-Montiel, Á.; Duarte-Mermoud, M.A.; Aguila-Camacho, N.; Contreras-Jara, C.; Álvarez Gracia, A. New Adaptive High Starting Torque Scalar Control Scheme for Induction Motors Based on Passivity. *Energies* **2020**, *13*, 1276. [CrossRef]
16. Travieso-Torres, J.C.; Contreras-Jara, C.; Diaz, M.; Aguila-Camacho, N.; Duarte-Mermoud, M.A. New Adaptive Starting Scalar Control Scheme for Induction Motor Variable Speed Drives. *IEEE Trans. Energy Convers.* **2022**, *37*, 729–736. [CrossRef]
17. Travieso-Torres, J.C.; Duarte-Mermoud, M.A. Normalized Model Reference Adaptive Control Applied to High Starting Torque Scalar Control Scheme for Induction Motors. *Energies* **2022**, *13*, 1276. [CrossRef]
18. Narendra, K.; Annaswamy, A. *Stable Adaptive Systems*; Dover Books on Electrical Engineering; Dover Publications: New York, NY, USA, 2012
19. Travieso-Torres, J.C.; Duarte-Mermoud, M.; Sepúleveda, D. Passivity-based control for stabilization, regulation and tracking purposes of a class of nonlinear systems. *Int. J. Adapt. Control. Signal Process.* **2007**, *21*, 582–602. [CrossRef]
20. Dini, P.; Saponara, S. Design of Adaptive Controller Exploiting Learning Concepts Applied to a BLDC-Based Drive System. *Energies* **2020**, *13*, 2512. [CrossRef]
21. Travieso-Torres, J.C.; Duarte-Mermoud, M.A.; Estrada, J.L. Tracking control of cascade systems based on passivity: The non-adaptive and adaptive cases. *ISA Trans.* **2006**, *45*, 435–445. [CrossRef]
22. Ganesan, S.; David, P.W.; Balachandran, P.K.; Samithas, D. Intelligent Starting Current-Based Fault Identification of an Induction Motor Operating under Various Power Quality Issues. *Energies* **2021**, *14*, 304. [CrossRef]
23. Park, R.H. Two-reaction theory of synchronous machines generalized method of analysis-part I. *Trans. Am. Inst. Electr. Eng.* **1929**, *48*, 716–727. [CrossRef]
24. O'Rourke, C.J.; Qasim, M.M.; Overlin, M.R.; Kirtley, J.L. A Geometric Interpretation of Reference Frames and Transformations: dq0, Clarke, and Park. *IEEE Trans. Energy Convers.* **2019**, *34*, 2070–2083. [CrossRef]
25. Mandic, D.P.; Kanna, S.; Xia, Y.; Moniri, A.; Junyent-Ferre, A.; Constantinides, A.G. A Data Analytics Perspective of Power Grid Analysis-Part 1: The Clarke and Related Transforms [Lecture Notes]. *IEEE Signal Process. Mag.* **2019**, *36*, 110–116. [CrossRef]
26. Holmes, D.; Lipo, T. *Pulse Width Modulation for Power Converters: Principles and Practice*; IEEE Press Series on Power and Energy Systems; Wiley-IEEE Press: Hoboken, NJ, USA, 2003.
27. Holtz, J. Pulsewidth modulation for electronic power conversion. *Proc. IEEE* **1994**, *82*, 1194–1214. [CrossRef]